The Astrophysical Journal, 619:1028–1035, 2005 February 1

X-RAY REFLECTION FROM INHOMOGENEOUS ACCRETION DISKS. II. EMISSION-LINE VARIABILITY AND IMPLICATIONS FOR REVERBERATION MAPPING

D. R. Ballantyne,[1] N. J. Turner,[2] and A. J. Young[3]

Received 2004 June 1; accepted 2004 October 7

ABSTRACT

One of the principal scientific objectives of the upcoming *Constellation-X* mission is to attempt to map the inner regions of accretion disks around black holes in Seyfert galaxies by reverberation mapping of the Fe Kα fluorescence line. This area of the disk is likely to be radiation pressure dominated and subject to various dynamical instabilities. Here, we show that density inhomogeneities in the disk atmosphere resulting from the photon bubble instability (PBI) can cause rapid changes in the X-ray reflection features, even when the illuminating flux is constant. Using a simulation of the development of the PBI, we find that for the disk parameters chosen, the Fe Kα and O VIII Lyα lines vary on timescales as short as a few hundredths of an orbital period. In response to the changes in accretion disk structure, the Fe Kα equivalent width (EW) shows variations as large as $\sim$100 eV. The magnitude and direction (positive or negative) of the changes depends on the ionization state of the atmosphere. The largest changes are found when the disk is moderately ionized. The O VIII EW varies by tens of eV and exhibits plenty of rapid, low-amplitude changes. This effect provides a natural explanation for some observed instances of short-timescale Fe Kα variability that was uncorrelated with the continuum (e.g., Mrk 841). New predictions for Fe Kα reverberation mapping should be made that include the effects of this accretion disk–driven line variability and a variable ionization state. Reflection spectra averaged over the evolution of the instability are well fitted by constant-density models in the 2–10 keV region.

Subject headings: accretion, accretion disks — instabilities — line: formation — radiative transfer — X-rays: general

1. INTRODUCTION

Shortly after the prediction of relativistically broadened iron Kα fluorescence lines in the X-ray spectra of accreting black holes (Fabian et al. 1989), it was realized that if the lines were variable, then constraints on the emission geometry and basic black hole parameters could be determined (Stella 1990; Matt & Perola 1992). These ideas matured into the prospect of iron line "reverberation mapping," which, given a series of short time–resolved X-ray spectra following a significant flare in the continuum, could accurately derive such fundamental parameters as the black hole mass, spin, and location of the X-ray source(s) (Reynolds et al. 1999; Young & Reynolds 2000; Ruszkowski 2000; Goyder & Lasenby 2004). The promise of this technique is such that iron line reverberation mapping of nearby Seyfert 1 galaxies is one of the principal science goals of the upcoming *Constellation-X* observatory.

In recent years it has become obvious that reverberation mapping will be more challenging than perhaps was previously thought. The *XMM-Newton* telescope has found only a handful of relativistically broadened Fe Kα lines, which indicates that these components may be in general quite weak, low-contrast features. Moreover, the best example of a relativistic line (observed from MCG $-$6-30-15; Fabian et al. 2002) exhibits less variability than the X-ray continuum and shows no correlation with the observed broadband flux (Vaughan & Edelson 2001; Vaughan & Fabian 2004; but see Ponti et al. 2004). These properties seem to apply on long timescales in a wide sample of bright Seyfert 1 galaxies (Weaver et al. 2001; Markowitz et al. 2003), but there also have been instances of rapid iron line variation with only a slight continuum change (Mrk 841; Petrucci et al. 2002) and in which the line at least partially follows the continuum (e.g., Nandra et al. 1997; Iwasawa et al. 2004). Clearly, there is a wide range of possible Fe Kα variability characteristics.

The problem that these observations cause with the standard reverberation picture is with the underlying assumption that variations in the Fe Kα line are directly related to changes in the observed continuum. The observed behavior shows that this assumption cannot be valid at all times and that there are other effects that are equally important to the production of the Fe Kα line. One possible perturbation of the previous reverberation calculations is photoionization of the accretion disk surface by the incident X-rays (the work by Reynolds et al. [1999], e.g., assumed only neutral reflection from the disk outside of the innermost stable circular orbit). If the disk surface is ionized to a certain level, then the Fe Kα equivalent width (EW) becomes anticorrelated with the continuum, in contrast to the positive correlation expected if the disk remains neutral (Nayakshin 2000; Ballantyne et al. 2002; Ballantyne & Ross 2002). It is also possible that the X-ray continuum incident on the disk is different from the observed one. For example, light-bending effects could enhance the illumination (Miniutti & Fabian 2004), while an outflowing corona could diminish it (Beloborodov 1999). While these effects may all be operating at some level, they are still connected with the X-ray continuum, and therefore a relation (positive or negative; strong or weak) between the Fe Kα line flux and the incident continuum is expected. In this paper, we outline a process by which the Fe Kα line can vary independently of the illuminating X-ray flux.

[1] McLennan Labs, Canadian Institute for Theoretical Astrophysics, 60 St. George Street, Toronto, ON, M5S 3H8, Canada; ballantyne@cita.utoronto.ca.
[2] Jet Propulsion Laboratory, California Institute of Technology, MS 169-506, Pasadena, CA 91109; neal.turner@jpl.nasa.gov.
[3] Center for Space Research, Massachusetts Institute of Technology, 77 Massachusetts Avenue, Cambridge, MA 02139; ayoung@space.mit.edu.

For systems accreting at greater than 0.3% of the Eddington rate, the innermost annuli of the accretion disk, where the relativistic portion of the iron Kα line is produced, are likely to be radiation pressure dominated (Shakura & Sunyaev 1973). Numerical results indicate that turbulence driven by the magnetorotational instability (MRI; Balbus & Hawley 1991) may involve large density fluctuations in radiation-dominated disks if the magnetic pressure exceeds the gas pressure and photons diffuse from compressed regions (Turner et al. 2003; Turner 2004). Large density variations may also be caused by the photon bubble instability (PBI; Arons 1992; Gammie 1998), which may develop into a series of shocks propagating through the plasma (Begelman 2001). These results suggest that radiation-dominated disks have time-varying density inhomogeneities on scales smaller than the disk thickness. In the first paper of this series (Ballantyne et al. 2004, hereafter Paper I), we showed that density variations in the outermost few Thomson depths can lead to reflection spectra differing from those of uniform slabs. Here, we continue our investigation of X-ray reflection from inhomogeneous accretion disks by computing the evolution of the reflection spectrum as the disk structure is changing as a result of the PBI. As is shown below, the changing density structure in the disk can affect the EW and line flux of the predicted emission lines, despite the constant illuminating continuum.

Section 2 details the setup and conditions of the PBI model and reflection calculations. We then present the results of the reflection models, both as a function of time and as time-averaged spectra (§ 3). The results are then discussed in § 4 before we summarize and draw our conclusions in § 5.

2. MODELS: SETUP AND CALCULATIONS

An important timescale in X-ray reflection is the time for the accretion disk to reestablish hydrostatic balance following a change in illumination (Nayakshin & Kazanas 2002; Collin et al. 2003). The adjustment time is approximately equal to the orbital period (Frank et al. 2002). Turbulence inside the disk results from the MRI and also has a characteristic overturn time similar to the orbital period (Balbus & Hawley 1998). In radiation-dominated disks, the PBI may grow faster than the orbital frequency (Blaes & Socrates 2003) and could lead to structures that vary over a small fraction of an orbit. Below, we examine time variations in the X-rays reflected from structures produced by the growth of photon bubbles. The variations are computed in two steps, as in Paper I. First, density distributions resulting from the instability are found using a two-dimensional, time-dependent numerical radiation-magnetohydrodynamic (MHD) calculation. The density profile along a single ray passing vertically through the disk is used as the input for the second step. We assume that X-rays from a diffuse external source strike the disk and calculate the reflected spectrum by solving the coupled equations of radiative transfer and ionization balance in one spatial dimension. The effects of changes in the density profile are tracked by calculating the spectrum 100 times per orbital period.

The calculation of the growth of photon bubbles is similar to that described in Paper I. A narrow annulus of accretion disk in orbit around a black hole of $M_{\rm BH} = 10^8\ M_\odot$ at a distance $R = 20R_{\rm S}$ (where $R_{\rm S} = 2GM_{\rm BH}/c^2$ is the Schwarzschild radius) is modeled in locally Cartesian coordinates in two dimensions, with symmetry assumed along the orbit. The frequency-averaged equations of radiation MHD are integrated using the ZEUS code (Stone & Norman 1992a, 1992b) with its flux-limited radiation diffusion module (Turner & Stone 2001) on a grid of 128×768 uniformly spaced zones. The initial condition is a Shakura-Sunyaev model with an accretion rate 10% of the Eddington limit for 10% radiative efficiency and an accretion stress parameter $\alpha = 0.06$. The total Thomson optical depth is 9200. To this is added a uniform magnetic field with a pressure 1% of the midplane radiation pressure, inclined 12° from horizontal. The initial state is disturbed slightly by applying random density perturbations of up to 1% in each grid zone. The domain extends 1.2 Shakura-Sunyaev semithicknesses to either side of the midplane and has a width of one sixth of the height. The horizontal boundaries are periodic, and the vertical boundaries allow gas, radiation, and magnetic fields to flow out but not in. Differential rotation is neglected, so there is no MRI and no external energy source. The radiation initially present escapes through the top and bottom boundaries, and the gas cools over time. The flux of radiation energy leaving each face of the disk initially is $F_{\rm disk} = 7.7 \times 10^{13}$ ergs cm^{-2} s^{-1}. During the first 0.8 orbits of the calculation, photon bubbles grow to nonlinear amplitudes and develop into trains of shocks. Photons then diffuse faster through the low-density regions between the shocks, and the disk flux is several times greater than it was initially. By 2.35 orbits, three quarters of the initial radiation energy is lost, and the horizontally averaged disk thickness is reduced by approximately half. A density floor of 1% of the initial midplane value or 9.93×10^{-12} g cm^{-3} is imposed during the calculation so that results are obtained with a reasonable amount of computer time. The floor is applied in the regions between shocks, reducing the overall density contrast. The dynamical time for this radius is $t_{\rm dyn} \sim (R^3/GM_{\rm BH})^{1/2} \sim \sqrt{8}(R/R_{\rm S})^{3/2} GM_{\rm BH}/c^3 \sim 1.2 \times 10^5 (R/20R_{\rm S})^{3/2} (M_{\rm BH}/10^8\ {\rm M}_\odot)$ s. The orbital period is 7.8×10^5 s, or about 9 days. The density profile along a ray passing vertically through the domain center is stored every 0.01 orbits for use in the X-ray reflection calculations.

Each density profile was trimmed so that the total Thomson depth through the gas was about 10. The number of zones in the density cuts varied from a minimum of 23 to a maximum of 71. Reflection spectra were then computed for each profile using the code described by Ross & Fabian (1993; see also Ballantyne et al. 2001). The illuminating continuum was a power law defined between 1 eV and 100 keV with a photon index $\Gamma = 2$. The gas was allowed to come into thermal and ionization balance before the reflection spectrum was computed (these timescales are generally much shorter than the hydrostatic time; e.g., Nayakshin & Kazanas 2002). The following ions are included in the calculations: C V–VII, N VI–VIII, O V–IX, Mg IX–XIII, Si XI–XV, and Fe XVI–XXVII. Four different illuminating fluxes $F_{\rm X}$ were used for each density profile in order to investigate differences due to ionization effects. These fluxes corresponded to $F_{\rm X}/F_{\rm disk} = 0.5$, 1, 4, and 8. Here, $F_{\rm disk}$ corresponds to the initial disk flux, and $F_{\rm X}$ does not change with time. All 944 ionized reflection models converged with no problems.

Of course, this procedure is not self-consistent, as the heating due to the illuminating X-rays is not included in the gas-dynamics. Similarly, the internal radiation field in the MHD calculation does not change the ionization state of the gas, nor is it included in the outgoing spectrum. Unfortunately, time-dependent two- and three-dimensional calculations of an X-ray–illuminated accretion disk with ionization physics, frequency-dependent radiative transfer, and MHD are still years away. However, we expect that the omissions described above do not greatly affect our results. The internal radiation field has temperatures of $\sim 10^5$ K, so neglecting its ionizing power does not affect the high-energy spectrum that is the focus of this paper. Ignoring the effects of X-ray heating on the gas structure is more problematic, as an optically thick skin may form on

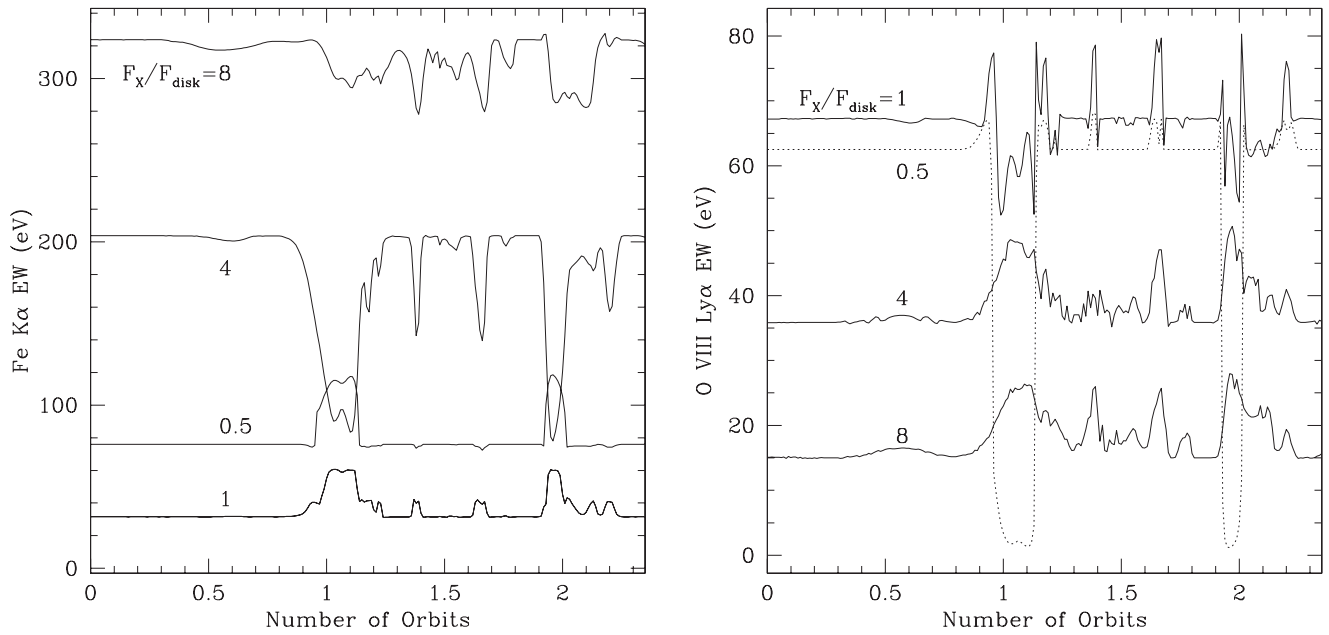

FIG. 1.—Evolution of the Fe Kα and O VIII Lyα EWs as the photon bubble simulation runs over 2.35 orbits. The $\Gamma = 2$ power law was added to the reflection spectra before the EW was calculated. The Fe Kα EW exhibits variability over timescales as small as a few hundredths of an orbit and can change by factors up to 2.5. The large drop of the O VIII EW when $F_X/F_{disk} = 0.5$ is due to increases in density causing significant absorption of the reflection spectrum.

the disk surface in hydrostatic models with $F_X/F_{disk} > 1$ (e.g., Nayakshin et al. 2000). This skin would then scatter and smear out the reflection spectrum. However, the return to hydrostatic balance after a pressure perturbation takes about an orbit, so the MRI and PBI may cause permanent disequilibrium. The turbulence driven by the MRI can lead to density changes in the gas on timescales of the orbital period (Turner et al. 2003) and can mix irradiated gas in to large optical depths. The fastest photon bubble modes have growth times shorter than the orbital period by the square root of the ratio of radiation to gas pressure. This estimate follows from Table 2 of Blaes & Socrates (2003) if the radiation and magnetic pressures exceed the gas pressure, as in the surface layers in a three-dimensional radiation-MHD calculation of a small patch of disk that includes the generation and buoyancy of the magnetic fields (Turner 2004). Furthermore, in the numerical photon bubble calculation described at the start of this section the instability leads to a radiative flux with a horizontal component comparable to the vertical one. The horizontal flux varies across the face of the disk, so the atmosphere feels substantial differential stresses. As is seen below, the densities change over periods as short as a few percent of an orbit, and the gas is out of hydrostatic balance from the time the instability reaches nonlinear amplitudes until the end of the calculation. These results suggest that like the disk itself, any X-ray–heated skin is inhomogeneous and time variable. The effects of irradiation on a turbulent atmosphere may be worth investigating with future calculations.

3. REFLECTION RESULTS

3.1. *Time-dependent Variations*

To quantify any changes made to the reflection spectra by the evolution of the PBI, we calculated the Fe Kα and O VIII Lyα EWs from each spectrum. Since the $\Gamma = 2$ power law will also be observed along with the reflection component, the two spectra were summed before the EW calculations were performed. The results are shown in Figure 1, with the different lines denoting the different values of F_X/F_{disk}. The Fe Kα EW spans the range from 20 to 60 eV when $F_X/F_{disk} = 1$ and the line is suppressed due to Auger destruction (Ross et al. 1996), but is $\sim$320 eV when $F_X/F_{disk} = 8$ and a strong ionized line at 6.7 keV is present. The plots show that there was little variation in the EWs of the emission lines over the first orbit, but large changes occurred afterward as the PBI grew in magnitude. A very significant variation in the Fe Kα EW occurred between orbits 0.9 and 1.2, where the density at the outermost layers of the atmosphere increased by $\sim$50%. Despite the small size of the increase in density, it greatly altered the Fe Kα EW, particularly when the line originated from ionized iron (i.e., when $F_X/F_{disk} = 4$). In that case, the Fe Kα EW dropped by a factor of $\sim$2.5 because of a decrease of the effective ionization parameter and an increase of the continuum absorption. On the other hand, when a neutral 6.4 keV line dominated or when the atmosphere was very highly illuminated, the small increase in density between orbits 1.0 and 1.1 caused much smaller changes in the Fe Kα EW (20–40 eV).

As mentioned in § 2, a density floor equivalent to 4.25×10^{12} cm^{-3} was used in the PBI simulation. Tests with a floor artificially lowered by a factor of 10 resulted in a more ionized reflection spectrum, as if F_X had been increased and the density was left unchanged. We conclude that the density floor will not qualitatively affect the results presented in Figure 1.

As an illustration of the rapidity of the possible changes to the reflection spectrum, Figure 2 plots the model spectra between 0.01 and 20 keV for every 0.01 of an orbit between orbits 1.6 and 1.69. The illuminating flux is $F_X/F_{disk} = 4$, and, as seen in Figure 1, the Fe Kα EW drops and recovers by $\sim$60 eV over this range. The inset in each panel shows the hydrogen number density (n_H) profile used in the reflection calculation and the equilibrium gas temperature found from the model. These plots illustrate that the density profile in the outer 10 Thomson depths of the accretion disk can change significantly over as little as 0.01 of an orbit. Some of the changes affect the reflection spectra, and some of them do not (depending on how strongly the

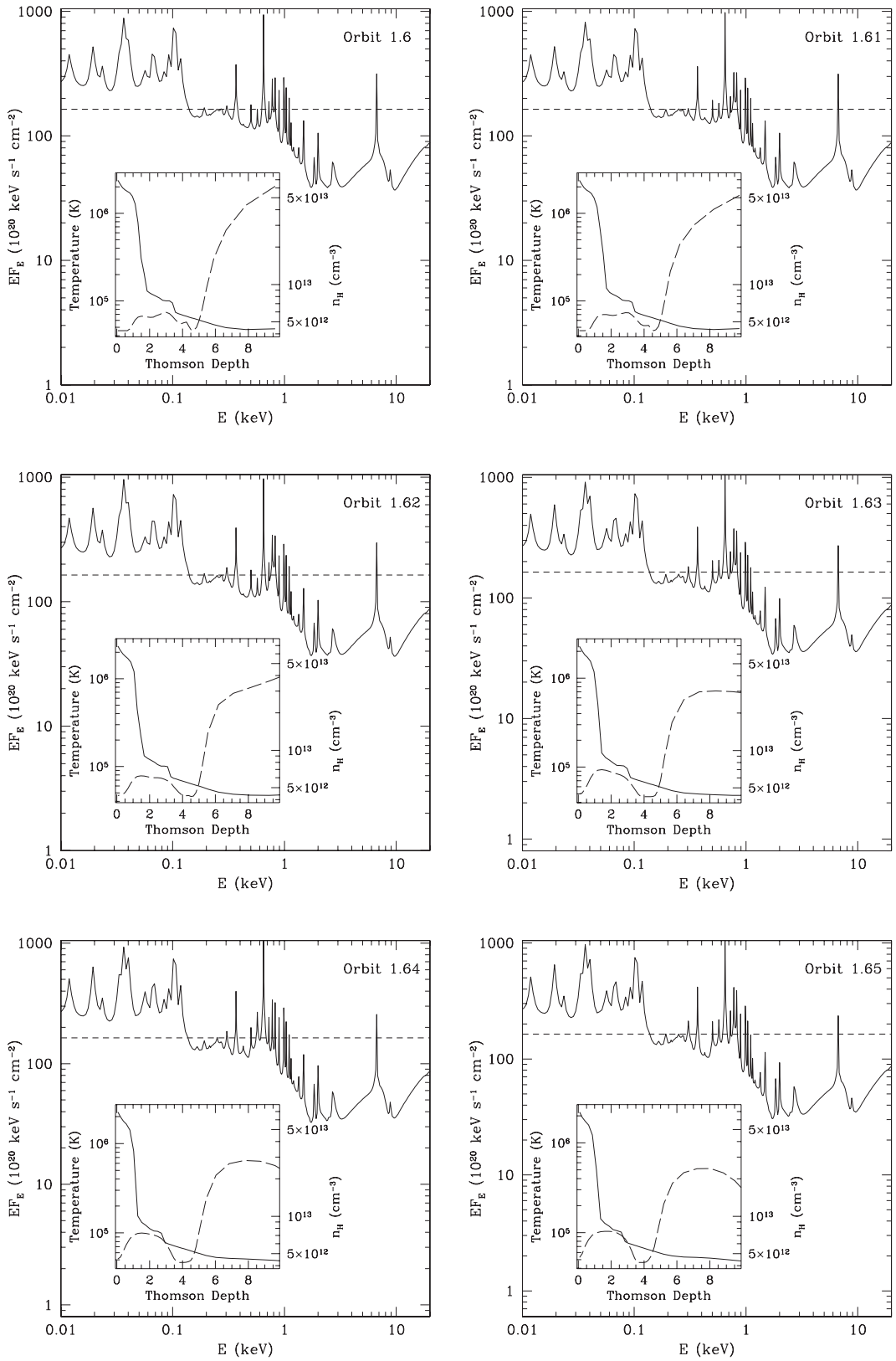

FIG. 2.—X-ray reflection spectra (*solid lines*) calculated from the outer 10 Thomson depths of a photon bubble simulation when $F_X/F_{disk} = 4$. The short-dashed lines denote the $\Gamma = 2$ power law that was incident on the material. The insets show the gas temperature (*solid lines*) and number density (*dashed lines*) for each model. The different plots show how the reflection spectra, temperature, and density changed as the simulation evolved from orbit 1.6 to orbit 1.69.

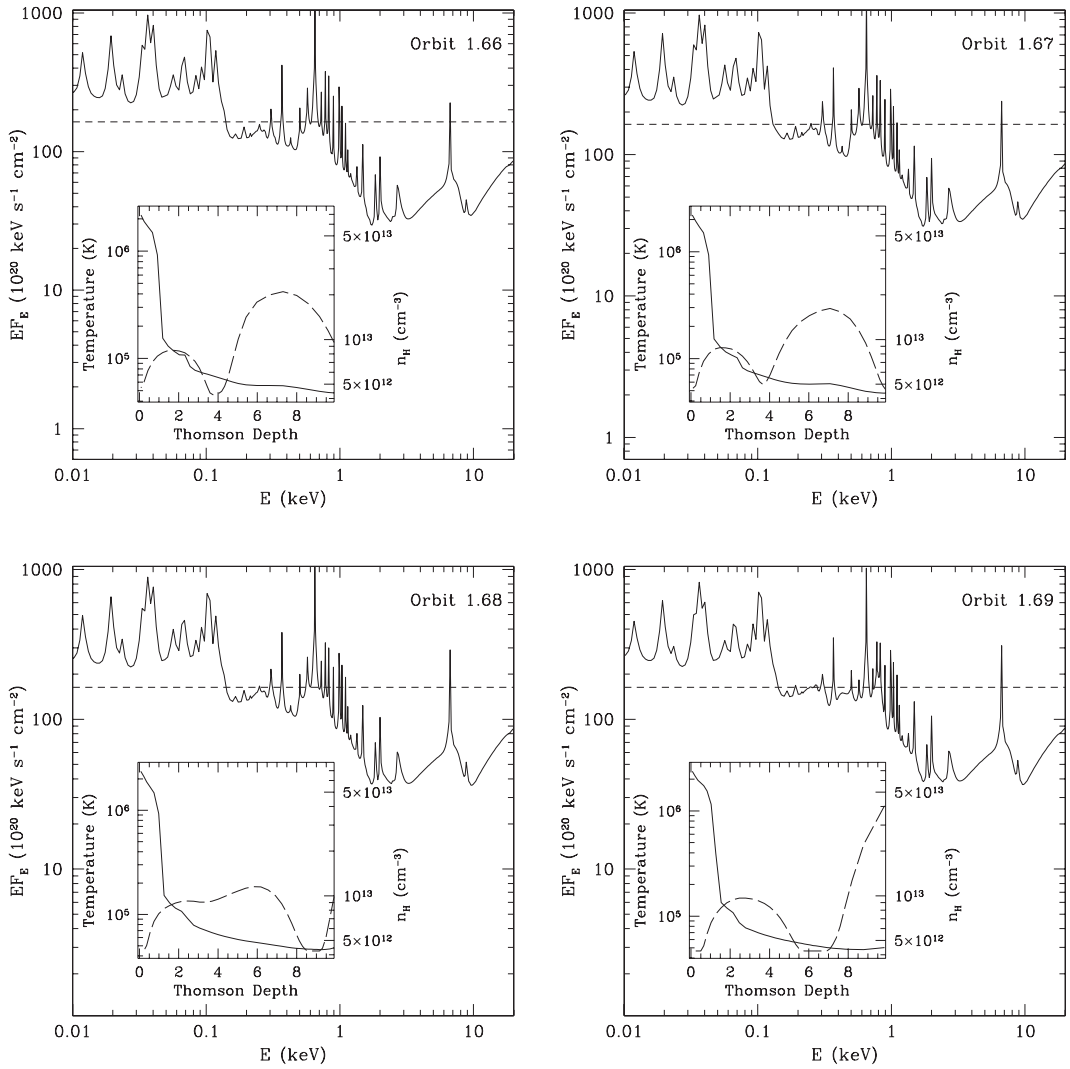

FIG. 2.—*Continued*

atmosphere is photoionized). However, in this case a rapid increase in density at the surface of the atmosphere caused a significant variation in the strength of the predicted Fe Kα line.

The second region of large-amplitude line variability takes place about a full orbit after the first instance, between orbits 1.9 and 2.2. The density at the outer part of the atmosphere increased rapidly (over only 0.06 orbits) as a shock front propagated diagonally along the magnetic field lines into the ray that we are considering. The resulting changes in the density structure as the shock passes through the ray result in the Fe Kα EW varying drastically and showing slight oscillatory behavior ($F_{\rm X}/F_{\rm disk} = 1$). We have thus clearly shown that changes in the accretion disk structure can cause rapid variability in the Fe Kα EW, *despite the continuum remaining constant*.

The right panel in Figure 1 illustrates the changes to the O VIII Lyα line resulting from the evolution of the PBI. The line, of course, is weaker when the disk is more highly ionized at large $F_{\rm X}/F_{\rm disk}$. The density enhancements that pass through the surface of the disk after about one orbit decrease the local ionization parameter and increase the O VIII EW, often by >10 eV, except for $F_{\rm X}/F_{\rm disk} = 1$ and 0.5. In these cases the increase in density makes it difficult for the weak continuum to ionize much oxygen, resulting in enhanced continuum absorption that suppresses the low-energy reflection spectrum. In these cases, the O VIII EW will be (sometimes drastically) reduced. Unlike the Fe Kα line, the O VIII EW exhibits small-amplitude, rapid variability between orbits 1 and 2. This is because the soft X-ray lines are very sensitive to where the illuminated gas is most rapidly cooling. As a result, the strength of the O VIII line, as well as those of the N VII and C VI lines, are more sensitive to the density structure than the Fe Kα line (see also Paper I).

Since the EW is a measure of the line strength relative to the continuum and the illuminating continuum is held constant in these calculations, the variations in both the Fe Kα and O VIII EWs are entirely due to intrinsic changes in the line flux in the reflection spectrum. Therefore, measurements of the line flux would also see changes of similar magnitude due to this effect.

3.2. *Time-averaged Spectra*

The variations presented above occurred on timescales as short as a few hundredths of an orbit, or $\sim$5–10 ks for the radius and black hole mass assumed for the simulation. This time is too short to accumulate a high-quality spectrum with modern observatories such as *XMM-Newton* and *Chandra*, except for the brightest Seyfert 1 galaxies. Typical observations need to be many times longer for proper spectral analysis, which will average over any variations in the emission lines due to the changing accretion disk structure. Thus, it is interesting to check

TABLE 1

Results of Fitting the Time-averaged Photon Bubble Reflection Spectra with Constant-Density Models

	0.2–12 keV				2.0–10 keV				
F_X/F_{disk}	Γ	ξ	R	χ^2/dof	Γ	ξ	R	χ^2/dof	$\tilde{n}_H$
0.5	2.012 ± 0.002	126 ± 0.3	$1.021^{+0.014}_{-0.011}$	3832/2358	$2.017^{+0.013}_{-0.012}$	74^{+13}_{-10}	$0.891^{+0.101}_{-0.091}$	1717/1595	6.5×10^{12}
1	$2.005^{+0.003}_{-0.002}$	249 ± 10	$0.993^{+0.013}_{-0.012}$	2706/2358	2.008 ± 0.010	219^{+51}_{-36}	$0.889^{+0.112}_{-0.109}$	1714/1595	4.4×10^{12}
4	$1.977^{+0.003}_{-0.002}$	697^{+10}_{-11}	$1.109^{+0.020}_{-0.019}$	3814/2358	$2.022^{+0.010}_{-0.011}$	964^{+50}_{-43}	$0.856^{+0.061}_{-0.063}$	1615/1595	4×10^{12}
8	$1.997^{+0.002}_{-0.001}$	$1122^{+0.3}_{-18}$	$0.837^{+0.010}_{-0.017}$	3432/2358	$2.024^{+0.008}_{-0.010}$	1738^{+185}_{-182}	$0.912^{+0.047}_{-0.049}$	1554/1595	4.45×10^{12}

Notes.—Averaged between 0.8 and 2.35 orbits. The normalizations of the photon bubble models were chosen so that the "observed" 2–10 keV flux was $(3-4) \times 10^{-8}$ ergs cm^{-2} s^{-1}. The reflection fraction R is defined as total = incident + $R \times$ reflected, and dof = degrees of freedom. The ionization parameter $\xi = 4\pi F_X/n_H$ has units of ergs cm s^{-1}, and $\tilde{n}_H$ is the density derived from the known F_X and fitted ξ. It has units of cm^{-3}. The error bars are the 2 σ uncertainty for the parameter of interest. The simulated data were constructed using the *XMM-Newton* response matrix *epn_sw20_sdY9.rmf* and assumed an exposure time of 40 ks.

whether the time-averaged spectra presented in § 3.1 retain any information about the unstable disk structure.

We follow very similar procedures to those described in Paper I. For each value of F_X/F_{disk}, we averaged together 156 reflection spectra between orbits 0.8 and 2.35 (in order to concentrate on the region in which the PBI is most important) and simulated a 40 ks *XMM-Newton* observation[4] with XSPEC ver. 11.3.0p (Arnaud 1996). The $\Gamma = 2$ power law was added to each averaged reflection spectrum so that the reflection fraction R is unity. The simulated spectra were then fitted with reflection models computed by the same code assuming a constant density of $n_H = 10^{13}$ cm^{-3}. The results of the spectral fitting are shown in Table 1. The fits are generally acceptable in the 0.2–12 keV energy range but are greatly improved in the 2–10 keV band. As a result of their sensitivity to the density structure, the soft X-ray emission features caused most of the difficulty in fitting the 0.2–12 keV simulated data (see also Paper I). The worst reduced χ^2 obtained was for the $F_X/F_{disk} = 0.5$ model over the 0.2–12 keV band. The residuals to this fit are shown in Figure 3 and are due to the slab model incorrectly accounting for the soft X-ray emission lines. However, the high-energy continuum is well modeled by a uniform reflector. This exercise suggests that the density variations at the surface of the disk will not greatly affect the time-averaged reflection spectra above 2 keV (but see § 4.2). Moreover, constant-density reflection models will be useful to parameterize observed spectra with an ionization parameter and reflection strength, provided that the observing time is long compared to the fluctuation timescale in the disk.

[4] Strictly speaking, a 780 ks observation would be needed to observe a full orbit of this PBI simulation. However, since the normalization of the model is chosen so that Poisson noise never dominates, the actual length of the simulated observation does not change the results.

4. DISCUSSION

4.1. *Variable Reflection Features*

In Paper I we showed that density inhomogeneities in the surface layers of radiation-dominated accretion disks could

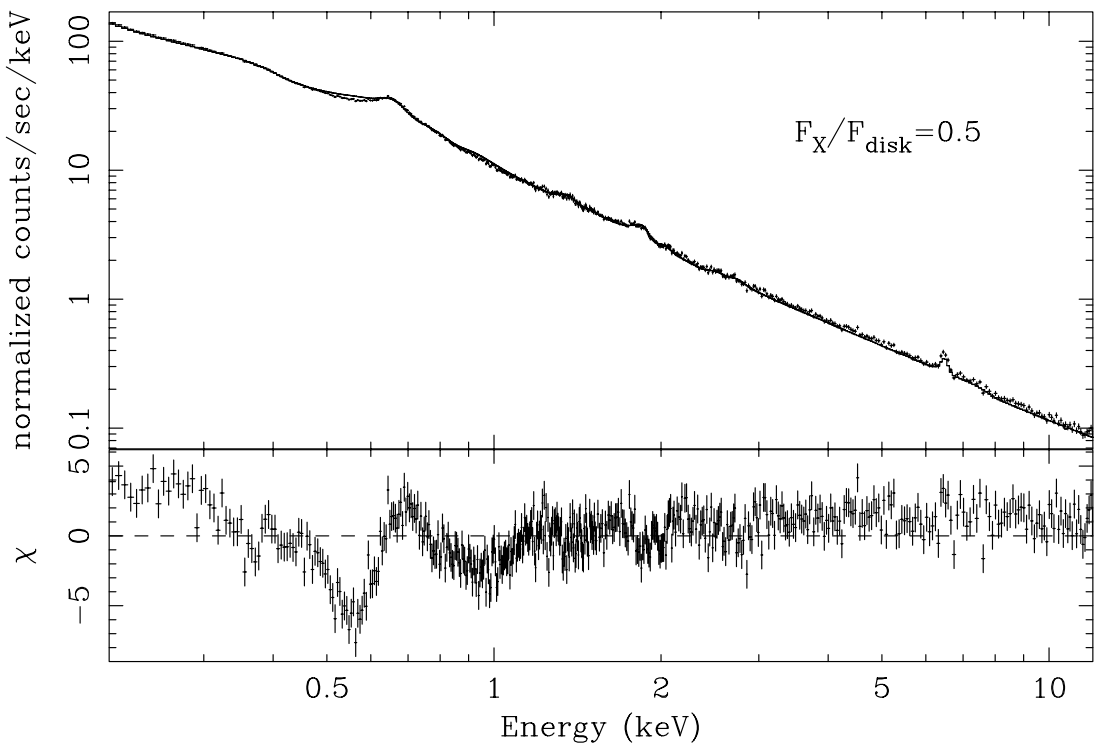

Fig. 3.—Simulated count spectra and residuals (in units of standard deviations) of the 0.2–12 keV constant-density fit to the time-averaged $F_X/F_{disk} = 0.5$ model. The fit parameters are given in Table 1.

potentially impact the reflection spectrum. That paper also suggested that the motion and evolution of any inhomogeneities in a real accretion disk might cause line variability that is independent of the illuminating radiation field. Here, we have confirmed that suggestion by explicitly showing variations in the Fe Kα and O VIII Lyα EWs on timescales as short as a few hundredths of an orbital period as a result of the evolution of the PBI, which is relevant for radiation-dominated accretion disks. This mechanism provides a natural explanation for any short-timescale Fe Kα variability that is uncorrelated with the continuum (e.g., Nandra et al. 1999; Wang et al. 2001). In particular, Figure 1 indicates that the sudden change in the Fe Kα EW observed in Mrk 841 (Petrucci et al. 2002) could easily be accounted for by changes in the accretion disk structure. Furthermore, as mentioned in Paper I, the narrow, redshifted lines that have been recently inferred in the spectra of NGC 3516 (Turner et al. 2002) and Mrk 766 (Turner et al. 2004) could originate in density inhomogeneities at a particular radius in the disk atmosphere. If this is the case, then our results indicate that the lines should be variable on timescales of about 1% of the orbital period of the emitting patch. While the statistics are generally poor, there is evidence for variability in these narrow lines. Future data will be able to provide a better test of this hypothesis.

The time-averaged reflection spectra from the PBI calculation showed no obvious indication of the variations on smaller timescales. However, we cannot rule out rapid variations in disk structure that produce iron Kα changes drastic enough to be detected in observations lasting several orbits. In this paper, we considered only one black hole mass, accretion rate, position in the disk, and magnetic field arrangement. For the parameters chosen, the Fe Kα region is readily fitted with a uniform-slab reflection model, while the soft X-ray region in some cases is not. Clearly, there is wide parameter space that needs to be explored in order to determine the full impact that the PBI and MRI will have on X-ray reflection spectra.

The results in § 3 have important implications for upcoming Fe Kα reverberation mapping attempts with *Constellation-X*. If accretion disk structural changes can cause the Fe Kα line to vary independently of the continuum on timescales much smaller than $t_{\rm dyn} \sim \sqrt{8}(R/R_{\rm S})^{3/2} GM_{\rm BH}/c^3$ ($\sim 1.2 \times 10^5$ s, for the photon bubble simulation shown here), then it will become an important source of noise for the reverberation experiments. This will be especially true for reverberation experiments probing small radii around low-mass black holes (say, $M_{\rm BH} \sim 10^{6-7}\, M_{\odot}$). In that case, the disk structure may vary on timescales as short as 100 s or less, comparable to the X-ray variability timescale (e.g., Vaughan et al. 2003). Furthermore, the current transfer functions computed for reverberation mapping have all neglected the effects of ionization of the disk surface (e.g., Reynolds et al. 1999), which can result in an anticorrelation between the line EW and continuum (Ballantyne & Ross 2002). Therefore, it is possible that the combined effects of a variable density structure (due to the PBI and perhaps other instabilities) and ionization state (due to changes in the X-ray illumination) will significantly complicate the results of any reverberation experiment. What is needed to provide concrete predictions for reverberation mapping is time-dependent ionized reflection calculations in which the illuminating flux is related to the underlying magnetic stress (e.g., Armitage & Reynolds 2003) or outgoing magnetic flux (Miller & Stone 2000). This is a direction for future research.

In the standard reverberation mapping scenario, the idea is to observe changes in the Fe Kα line as X-rays from a flare sweep across the disk. The PBI will likely be ongoing at every radius in the inner region of the disk but will be subject to local conditions, such as the strength and geometry of the magnetic field. Moreover, the linear growth rate of the PBI increases as one moves to smaller radii (Blaes & Socrates 2001). Therefore, the disk structure will be very position dependent as the X-rays flash overhead, so the reflection spectrum could show variability due to disk inhomogeneities as a function of position as well as time. PBI simulations spanning a larger range in radius would be necessary to test the possibility of reflection spectra variability due to positional changes.

If different radii produce different variability properties, then the observed variations may be diluted if the X-rays illuminate a wide enough range of radii. However, there are often times when the active galactic nucleus (AGN) continuum is likely to be dominated by a single flare or a number of small flares that occur in close proximity to one another (cf. Merloni & Fabian 2001). In this case, which is the most relevant for reverberation mapping, the one-zone models employed here may be useful.

The signature of a changeable disk atmosphere is, of course, short-timescale Fe Kα (and O VIII Lyα, if observable) variability that is independent of the observed continuum. Therefore, it may be possible to observationally test whether this process is important. As mentioned above, such cases of rapid changes in the Fe Kα line have been observed (e.g., Mrk 841), but these cannot be used as evidence that effects of disk instabilities have been observed (although they may provide a good explanation). There still remain too many unknowns regarding the location and dynamics of the X-ray source providing the illuminating continuum. The long-timescale disconnectedness between the Fe Kα line and continuum (e.g., Markowitz et al. 2003) suggests that it is possible, if not likely, that at some level the disk sees a different irradiating continuum than what is observed. Numerical simulations of coronal formation above accretion disks, still some years away, may provide the clues to understanding the X-ray source in AGNs.

4.2. *Implications of the Time-averaged Results*

The reflection spectra that were averaged over the variability caused by the PBI were well described by a constant-density model in the 2–10 keV band. The implication is that over this energy range, the spectrum is dominated by emission from a single ionization parameter. Since the illuminating flux is known for these test cases, the best-fit ξ can be used to determine $\tilde{n}_{\rm H} = 4\pi F_{\rm X}/\xi$, the density at which the most important spectral features are formed (see Table 1). The value of $\tilde{n}_{\rm H}$ is always less than 10^{13} cm^{-3}, the density actually used in the constant-density models, indicating that the ionization level is higher than "expected" given the illuminating flux. As can be seen in the density profiles plotted in Figure 2, $\tilde{n}_{\rm H}$ predominantly falls within the first 1–2 Thomson depths of the atmosphere. We conclude that reflection spectra above 2 keV are effectively determined by the ionization parameter at a Thomson depth of $\sim$1. At lower energies, the carbon, nitrogen, and oxygen cooling lines, which are very sensitive to the density structure, cause the spectra to exhibit features from different effective ionization parameters and thus are more difficult to fit with a uniform-density model.

The fits with the constant-density models suggest that changes in the calculated spectra on 0.01–0.1 orbit timescales are difficult to detect in the longer integrations. However, there may be regimes in which rapid changes in disk structure produce clear signatures in the Fe Kα region in observations lasting several orbits. As mentioned in § 4.1, we considered only one black hole mass, accretion rate, position in the disk, and magnetic field arrangement. Thus, there is a wide parameter space to be

explored to determine the impact of accretion disk inhomogeneities on X-ray reflection spectra. Nevertheless, insofar as can be determined, these results (along with those from Paper I) indicate that constant-density models provide a good indication of the average ionization state of the accretion disk atmosphere on long timescales.

5. CONCLUSIONS

Our conclusions from the second paper in our study on X-ray reflection from heterogeneous accretion disks can be summarized as follows:

1. Changes in the density structure of an accretion disk atmosphere from the photon bubble instability (PBI) can give rise to rapid variability of emission lines in the X-ray reflection spectrum. These variations would be observed to be independent of the illuminating continuum.

2. This process gives a natural explanation for any short-timescale (e.g., hours) line variability that seemed to be uncorrelated with the X-ray continuum (for example, Mrk 841). However, these observations cannot be used as proof that disk instabilities are causing the line variations, and this process cannot offer an explanation for the uncorrelated behavior of the Fe Kα line on longer timescales (greater than a day), although we can not rule out such an effect in a different region of parameter space.

3. The timescale of the variability was found to be as small as a few hundredths of an orbital period. Therefore, this effect, combined with any changes in ionization state, could be a serious source of noise for future reverberation studies.

4. Averaging the individual reflection spectra over the 1.55 orbits most affected by the PBI yielded spectra corresponding to the more common long-timescale X-ray AGN observations. These averaged spectra were well fitted above 2 keV by constant-density models.

5. Photon bubble structures move across the surface of the disk in the radiation-MHD calculations, passing in and out of the ray along which we extracted density profiles. Variations in the X-rays reflected from a region containing many structures may be less than those from a single line of sight. The separations, strengths, and orientations of the structures are found to vary with the alignment and strength of the magnetic fields. The fields are likely to evolve over orbital timescales along with the turbulence inside the disk. Two- and three-dimensional reflection calculations may be useful in studying the consequences for reverberation mapping.

The authors thank Omer Blaes for useful discussions and the referee for helpful comments that improved the paper. D. R. B. acknowledges financial support by the Natural Sciences and Engineering Research Council of Canada. N. J. T. was supported by a National Research Council fellowship at the Jet Propulsion Laboratory, California Institute of Technology. A. J. Y. was supported by NASA through contract NAS8-01129. This work was partly supported by US National Science Foundation grant AST-0307657.

REFERENCES

Armitage, P. J., & Reynolds, C. S. 2003, MNRAS, 341, 1041
Arnaud, K. A. 1996, in ASP Conf. Ser. 101, Astronomical Data Analysis Software and Systems V, ed. G. H. Jacoby & J. Barnes (San Francisco: ASP), 17
Arons, J. 1992, ApJ, 388, 561
Balbus, S. A., & Hawley, J. F. 1991, ApJ, 376, 214
———. 1998, Rev. Mod. Phys., 70, 1
Ballantyne, D. R., Fabian, A. C., & Ross, R. R. 2002, MNRAS, 329, L67
Ballantyne, D. R., & Ross, R. R. 2002, MNRAS, 332, 777
Ballantyne, D. R., Ross, R. R., & Fabian, A. C. 2001, MNRAS, 327, 10
Ballantyne, D. R., Turner, N. J., & Blaes, O. M. 2004, ApJ, 603, 436 (Paper I)
Begelman, M. C. 2001, ApJ, 551, 897
Beloborodov, A. M. 1999, ApJ, 510, L123
Blaes, O., & Socrates, A. 2001, ApJ, 553, 987
———. 2003, ApJ, 596, 509
Collin, S., Coupé, S., Dumont, A.-M., Petrucci, P.-O., & Różańska, A. 2003, A&A, 400, 437
Fabian, A. C., Rees, M. J., Stella, L., & White, N. E. 1989, MNRAS, 238, 729
Fabian, A. C., et al. 2002, MNRAS, 335, L1
Frank, J., King, A., & Raine, D. 2002, Accretion Power in Astrophysics (3rd ed.; Cambridge: Cambridge Univ. Press)
Gammie, C. F. 1998, MNRAS, 297, 929
Goyder, R., & Lasenby, A. N. 2004, MNRAS, 353, 338
Iwasawa, K., Lee, J. C., Young, A. J., Reynolds, C. S., & Fabian, A. C. 2004, MNRAS, 347, 411
Markowitz, A., Edelson, R., & Vaughan, S. 2003, ApJ, 598, 935
Matt, G., & Perola, G. C. 1992, MNRAS, 259, 433
Merloni, A., & Fabian, A. C. 2001, MNRAS, 328, 958
Miller, K. A., & Stone, J. M. 2000, ApJ, 534, 398
Miniutti, G., & Fabian, A. C. 2004, MNRAS, 349, 1435
Nandra, K., George, I. M., Mushotzky, R. F., Turner, T. J., & Yaqoob, T. 1999, ApJ, 523, L17
Nandra, K., Mushotzky, R. F., Yaqoob, T., George, I. M., & Turner, T. J. 1997, MNRAS, 284, L7
Nayakshin, S. 2000, ApJ, 540, L37
Nayakshin, S., & Kazanas, D. 2002, ApJ, 567, 85
Nayakshin, S., Kazanas, D., & Kallman, T. 2000, ApJ, 537, 833
Petrucci, P. O., et al. 2002, A&A, 388, L5
Ponti, G., Cappi, M., Dadina, M., & Malaguti, G. 2004, A&A, 417, 451
Reynolds, C. S., Young, A. J., Begelman, M. C., & Fabian, A. C. 1999, ApJ, 514, 164
Ross, R. R., & Fabian, A. C. 1993, MNRAS, 261, 74
Ross, R. R., Fabian, A. C., & Brandt, W. N. 1996, MNRAS, 278, 1082
Ruszkowski, M. 2000, MNRAS, 315, 1
Shakura, N. I., & Sunyaev, R. A. 1973, A&A, 24, 337
Stella, L. 1990, Nature, 344, 747
Stone, J. M., & Norman, M. L. 1992a, ApJS, 80, 753
———. 1992b, ApJS, 80, 791
Turner, N. J. 2004, ApJ, 605, L45
Turner, N. J., & Stone, J. M. 2001, ApJS, 135, 95
Turner, N. J., Stone, J. M., Krolik, J. H., & Sano, T. 2003, ApJ, 593, 992
Turner, T. J., Kraemer, S. B., & Reeves, J. N. 2004, ApJ, 603, 62
Turner, T. J., et al. 2002, ApJ, 574, L123
Vaughan, S., & Edelson, R. 2001, ApJ, 548, 694
Vaughan, S., & Fabian, A. C. 2004, MNRAS, 348, 1415
Vaughan, S., Fabian, A. C., & Nandra, K. 2003, MNRAS, 339, 1237
Wang, J.-X., Wang, T.-G., & Zhou, Y.-Y. 2001, ApJ, 549, 891
Weaver, K. A., Gelbord, J., & Yaqoob, T. 2001, ApJ, 550, 261
Young, A. J., & Reynolds, C. S. 2000, ApJ, 529, 101